J. Fluid Mech. (2008), *vol.* 608, *pp.* 197–215.
doi:10.1017/S0022112008002371 Printed in the United Kingdom

Effect of vorticity on steady water waves

JOY KO AND WALTER STRAUSS
Mathematics Department, Brown University, Box 1917, Providence, RI 02912, USA

(Received 15 October 2007 and in revised form 7 April 2008)

Two-dimensional, finite-depth periodic steady water waves with variable vorticity $\omega = \gamma(\psi)$ and large amplitude a are computed for a large number of cases. In particular, the effect of a shear layer at the top, the middle or the bottom is considered. The maximum amplitude a_{max} varies monotonically with the vorticity function $\gamma(\cdot)$. It is increasing if the stagnation point is at the crest, and is decreasing if the stagnation point is in the interior of the fluid or on the bottom. Relationships between the amplitude, hydraulic head, depth and mass flux are investigated.

1. Introduction

Evidence from experimental studies shows that qualitative features of water waves can be greatly affected by the presence of vorticity. However, numerical studies on rotational water waves have been almost entirely restricted to the simplified setting of constant vorticity. These studies have consistently shown that features such as the shape of the wave, the amplitude of the crest, and the presence of eddies differ from those found in the irrotational setting. There may be 'extreme' or 'breaking' waves with points of stagnation. They indicate the possibility of eddies or of overhanging wave profiles. The irrotational case is the only one for which there is a complete picture of an extreme wave. This is the extreme Stokes wave, for which the only point of stagnation is the crest with an angle of 120°. However, theoretical work concerning extreme rotational waves is quite sparse.

In the present work, we compute families of periodic water waves with variable vorticity and large amplitude. It is a continuation of Ko & Strauss (2008) in which our focus was the constant vorticity case. In the present paper, our main concern is the study of vorticities that are not constant. The vorticity can be completely arbitrary. A layer of non-zero vorticity can occur near the surface owing to the action of wind. Vorticity of an ocean wave near the shore can occur because of the topography of the bottom. A steady water wave is often a good model on a short time scale. We emphasize that our calculations make no shallowness or small-amplitude approximation.

We do assume that the water is incompressible and inviscid without surface tension, lies over a flat bottom, and is acted upon by gravity g. We assume that the waves are two-dimensional, periodic and of permanent form. Then the only remaining free parameters are the period $2L$, the Bernoulli constant Q (which is related to the hydraulic head, i.e. the energy of the wave), the relative mass flux p_0, the speed c of the wave, and of course the vorticity function $\gamma(\cdot)$ where $\omega = \gamma(\psi)$. The average depth d is determined implicitly in terms of the other parameters. We treat Q as a bifurcation parameter, thereby generating a one-parameter family of waves, for each choice of the other parameters. Each wave profile in the family has one crest and one

trough per period and is even around the crest. There are waves in the family that have points that approach stagnation.

Our principal aim is to investigate how the amplitude, shape, depth and stagnation points of a wave depend on the vorticity function γ, Bernoulli constant Q, and relative mass flux p_0. Our computations suggest that the family of waves is a continuous curve in function space. We will denote the computed family by $\mathscr{C}$. For brevity, we will subsequently refer to it as the 'bifurcating curve'. Our simulations are unable to generate waves with exact stagnation points, but we do approach stagnation. In this paper we will simply refer to such a situation as 'stagnation'. In our computations we always normalize the period to be 2π. Our computations yield the following results.

(i) For given γ and p_0, the amplitude a is an increasing function along the bifurcating curve $\mathscr{C}$. Therefore the maximum amplitude a_{max} occurs at the end of $\mathscr{C}$ (as far as the computation goes).

(ii) In every case we find that the stagnation point along $\mathscr{C}$ lies on the vertical line below the crest. In contrast to the irrotational case, stagnation occurs either at an interior point of the fluid or on the bottom directly below the crest if the vorticity is sufficiently large and positive.

(iii) As the vorticity is varied for a given p_0, the maximum amplitude a_{max} varies monotonically with the vorticity function $\gamma(\cdot)$. The location of the stagnation separates the cases of increasing and decreasing a_{max}. Specifically, if the stagnation point is located at the crest and $\gamma_1(p) \leqslant \gamma_2(p)$ for all p, then $a^1_{max} \leqslant a^2_{max}$. If the stagnation point occurs elsewhere and $\gamma_1(p) \leqslant \gamma_2(p)$ for all p, then $a^1_{max} \geqslant a^2_{max}$.

(iv) The maximum amplitude a_{max} is an increasing function of the magnitude of the flux $|p_0|$, in the case of constant vorticity.

(v) The depth d varies only slightly along each continuum for fixed flux p_0.

(vi) Generally, the hydraulic head, essentially Q, increases along the bifurcating curve $\mathscr{C}$ and then decreases as stagnation is approached at the crest. The turning point, where Q starts to decrease, moves closer to the end of the continuum as the vorticity function increases. On the other hand, if the stagnation occurs in the interior or at the bottom, then there may be no turning point.

We pay particular attention to vorticities that are non-zero in a surface layer and are zero (irrotational) below that layer (see § 3). Such a vorticity is a simple model of a wave under the influence of wind at the surface because the wind creates vorticity near the surface, as is well known. A favourable wind will produce negative vorticity, while an adverse wind will produce positive vorticity. Our results show that the maximum amplitude will occur for a relatively large positive vorticity. They also show that a favourable wind, which corresponds to negative vorticity, tends to make waves break sooner.

In § 4, we also consider a vorticity layer at the bottom, which could happen, for instance, near an ocean shore. Then we consider a middle shear layer, which is an example of a non-monotone vorticity function. Finally, we consider a continuous distribution, in order to emphasize that our results do not depend on the discontinuities of $\gamma(\cdot)$.

In this paper and Ko & Strauss (2008), we numerically follow the bifurcating curve $\mathscr{C}$ using the parameter Q. We do not use truncated Fourier modes, shallow-water or small-amplitude approximations. Instead, we solve the fully elliptic system that results from the Dubreil-Jacotin (DJ) transformation (see below) along the bifurcating curve, using standard finite differencing and nonlinear solvers, as well as the efficient numerical continuation library TRILINOS.

There is of course a huge literature concerning irrotational waves, especially in various small-amplitude and shallow-water approximations (Milne-Thomson 1996; Johnson 1997; Lighthill 2001). If the vorticity ω is a constant, we can introduce a pseudostreamfunction that is a harmonic function, in analogy with the irrotational case. Thus the Euler equations can be converted via the Cauchy integral theorem to a boundary-integral formulation. This formulation is relatively easy to solve numerically (but not theoretically). The first to use this approach were Simmen & Saffman (1985) who considered periodic waves with infinite depth and Teles da Silva & Peregrine (1988) who treated periodic waves with finite depth. Teles da Silva & Peregrine showed that eddies can form at the finite bottom directly below the crest if the vorticity is positive and large enough. If the vorticity is negative, an extreme wave can form with stagnation at the crest, but it does not have the same shape as in the irrotational case. Their key paper clearly shows that vorticity can have a profound effect on the shape of the wave.

Using the same method, Vanden-Broeck (1994, 1995) and Okamoto & Shoji (2001) computed various families of solitary waves with finite depth and constant vorticity, obtaining results consistent with those of Teles da Silva & Peregrine. Miroshnikov (2002) also considered solitary waves using the same basic formulation. However, in his work the water has to be shallow and the numerical method is based on several approximations including an expansion in powers of the depth. As Teles da Silva & Peregrine did, Miroshnikov found eddies forming at the bottom if the vorticity is positive, but, in direct contradiction to the results of both Teles da Silva & Peregrine and Vanden-Broeck, he also found eddies forming near the crest. Sha & Vanden-Broeck (1995) computed solitary waves in the case of a surface or bottom shear layer, but their waves are not periodic, they did not compute large families of waves, and they did not find any bottom or interior stagnation points.

A few papers have dealt with the case of variable vorticity. Dalrymple (1977) used a method based on the Dubreil-Jacotin transformation (see below), which permits the treatment of an arbitrary vorticity distribution but cannot treat overhanging waves. In fact, Dubreil-Jacotin (1934) had been the first to provide any theoretical analysis of waves with general vorticities. Dalrymple specified all the physical constants and therefore he computed only particular examples in each run. He computed just two particular examples in detail, one with constant vorticity and one with a vorticity satisfying a power law.

Thomas (1990) also used the Dubreil-Jacotin method similarly to Dalrymple, computing individual waves, but included a background current and performed the computation using truncated Fourier modes. Solitary waves in the presence of a background current had been considered by Benjamin (1962). Comparing his numerical results with experimental data, Thomas' key conclusion was that the vorticity does have a major influence on the nature of the wave.

Swan, Cummins & James (2001) undertook an experimental and numerical study of time-dependent waves propagating on a strongly sheared current with a non-constant vorticity distribution. They found, experimentally, that a negative vorticity distribution can have several main effects on the gross appearance of a wave. There may be greater crest–trough asymmetry (with a broader trough and a sharper crest). The wave may be steeper than in the irrotational case and thus the local acceleration of the water particles can be greater. Even if the vorticity is confined to the upper layers of the water, the flow is modified over the entire water depth. (Note that what Swan *et al.* call 'negatively sheared' is what we call 'positive vorticity', and vice versa.)

In order to fix our notation, we now write the governing equations in the moving frame for steady water waves travelling at speed c. They are

$$\begin{aligned} &\Delta\psi = -\gamma(\psi) && \text{in} \quad \{-d < y < \eta(x)\},\\ &|\nabla\psi|^2 + 2g(y+d) = Q && \text{on} \quad \{y = \eta(x)\},\\ &\psi = 0 && \text{on} \quad \{y = \eta(x)\},\\ &\psi = -p_0 && \text{on} \quad \{y = -d\}, \end{aligned}$$

where ψ is the relative streamfunction ($\psi_x = -v$, $\psi_y = u - c$), $\omega = \gamma(\psi)$ is the vorticity, $S = \{y = \eta(x)\}$ is the free surface, and $p_0 = \int_{-d}^{\eta(x)} (u-c)\,\mathrm{d}y < 0$ is the relative mass flux which is independent of x. The Bernoulli constant Q is given by $Q = 2(E + gd)$, where E is the hydraulic head of the flow. We assume that $u < c$ throughout the fluid and that the profile has period $2L$ in x, is even around the crest and is monotone from crest to trough. The DJ transformation $q = x$, $p = -\psi(x, y)$ has the effect of transforming the free-boundary problem given above into the boundary-value problem

$$\left.\begin{aligned} &\left(1 + h_q^2\right) h_{pp} - 2h_p h_q h_{pq} + h_p^2 h_{qq} = -\gamma(-p) h_p^3 && \text{in} \quad R,\\ &1 + h_q^2 + (2gh - Q) h_p^2 = 0 && \text{on} \quad p = 0,\\ &h = 0 && \text{on} \quad p = p_0, \end{aligned}\right\} \tag{1.1}$$

in the fixed rectangle $R = (-L, L) \times (p_0, 0)$ where the height above the flat bed $h(q, p) = y + d$ is even and has period $2L$ in the q-variable. We take $q = x = 0$ to correspond to the crest and $q = x = L$ to the trough. Note that the Jacobian of the transformation is $-\psi_y = c - u$.

Working with this reformulation (1.1) of the water-wave problem and using bifurcation and degree theory, the existence of a global connected set of smooth solutions was proved in Constantin & Strauss (2004), for any constant $c > 0$ and any smooth function γ, if $p_0 < 0$ is subject to a size restriction. This connected set contains both laminar ('trivial') flows and waves with the value of u arbitrarily close to the wave speed c at some point. A point where $u(x, y) = c$ is a stagnation point, which means that the Jacobian vanishes. Notice that the speed c is completely arbitrary as it does not appear explicitly in the mathematical formulation (1.1) of this finite-depth problem. For further details of the mathematical theory, see Okamoto & Shoji (2001), Constantin & Escher (2004), Constantin & Strauss (2004, 2007), Hur (2007) and Varvaruca (2008).

Details of our numerical procedure are given in Ko & Strauss (2008). In all our computations, with mks units in mind, we choose horizontal period $2L = 2\pi$ and $g = 9.8$. The horizontal mesh size M and the vertical mesh size N are chosen to be either $M = 250$, $N = 500$ or $M = N = 500$. For the sake of visibility, in the figures of waves (except figure 7) we have printed only every tenth streamline. The vertical axis for all the figures of the waves corresponds to the value of $y + d$; a value of 0 on this axis corresponds to the finite bottom $y = -d$. Since the Jacobian corresponding to our discretization is nearly singular close to stagnation, the step sizes in Q become increasingly small as we approach waves with a stagnation point. Our determination for whether a wave has a point near stagnation involves a careful calibration of the convergence tolerances for the solvers as well as the requirement that the minimum value of $c - u$ be less than 10 % of its value at the initially bifurcating wave. This modest criterion is based on extensive computations for two base cases in the constant vorticity setting, for which an extremely small fixed step size was used near stagnation. For these runs, we were able to push the minimum value of $c - u$ to 1 % of its initial

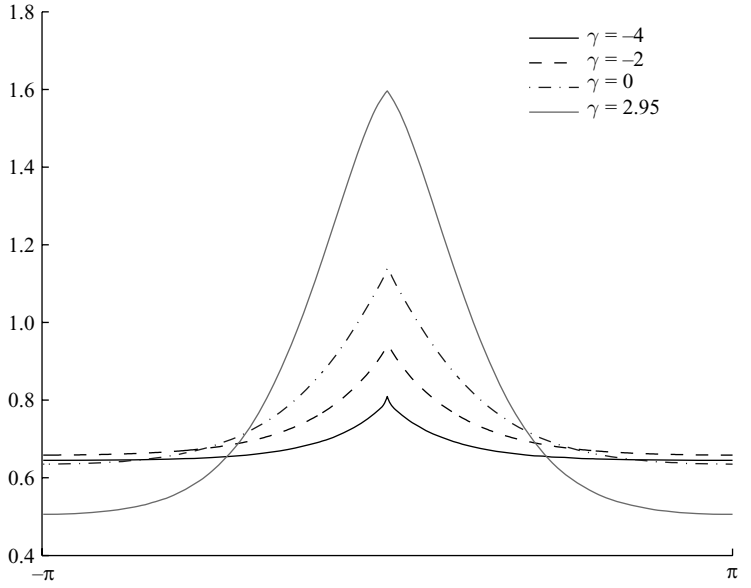

FIGURE 1. Waves near stagnation for four subcritical constant vorticities.

value with only a 3 % increase in the amplitude. These runs show that first-order accuracy is qualitatively correct, being a good approximation to the wave with a stagnation point.

In § 2, we treat the case of constant vorticity; in § 3, the case of surface shear; and in § 4, several other cases of variable shear. In § 5, we consider the behaviour of the waves as a function of the flux p_0.

2. Constant shear

In this section, we consider the case that the vorticity is a constant. This was also the focus of Ko & Strauss (2008), but since then we have investigated several additional properties.

One of the key observations in Ko & Strauss (2008) was that, given the relative mass flux p_0 and the period $2L$ of the wave, there is a critical value γ_{crit} of the vorticity that separates the cases for which the first stagnation occurs at the crest or on the bottom. For $L = 2\pi$, $g = 9.8$ and $p_0 = -2$, we found that $\gamma_{crit} \approx 2.96$. The streamlines are level curves of the velocity potential ψ. Vertical separation of two nearby streamlines occurs where $\psi_y = u - c$ is small, that is, near a stagnation point. Although we did not assume that stagnation could occur only at the crest A or the point B on the bottom just below the crest, we in fact found that our simulations produced only these two locations on the boundary as points of stagnation.

Moreover, we compared waves near stagnation with $p_0 = -2$ for various vorticities and found that vorticity influences the shapes of their profiles (figure 1). Positive vorticity leads to a sharper, higher crest, while negative vorticity leads to a lower, more localized crest.

Since Ko & Strauss (2008), we have further investigated the amplitude a of the crest and the average depth d. Our interest is in studying the amplitude and depth of the waves both along the bifurcating curve $\mathscr{C}$ and as a function of the vorticity. Figure 2 shows the values of a and d of the waves along $\mathscr{C}$ for four constant vorticities. Each

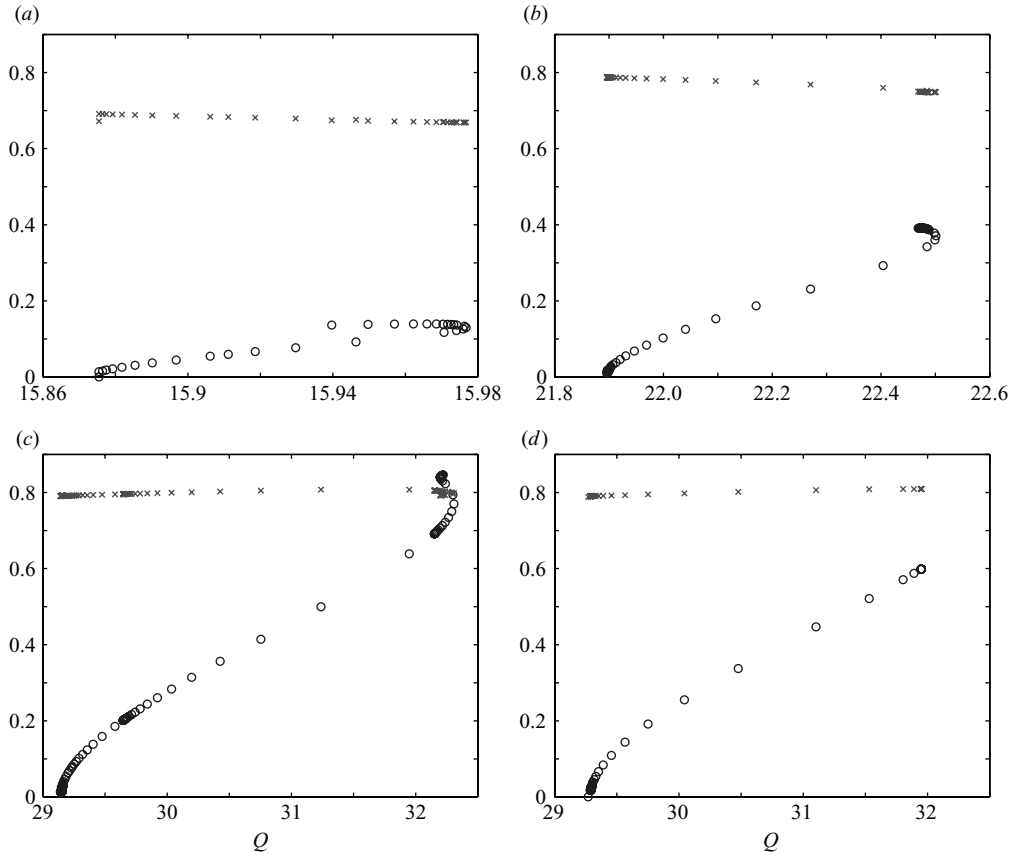

FIGURE 2. Amplitudes (○) and depths (×) of waves along the bifurcation curves for (*a*) $\gamma = -4$, (*b*) 0, (*c*) 2.95, (*d*) 3.

data point in the figure refers to a computed wave along the bifurcating curve. The spacing of the data points is uneven because the program takes adaptive step sizes in the bifurcation parameter Q according to a combination of an initial step size specified by the user and the stiffness of the Jacobian. We see from figure 2 that the data points are tightly clustered in the beginning of the bifurcation curve because the initial step size that is specified is very small, and again near stagnation since the Jacobian tends to become quite stiff near stagnation.

As for the depth d, in all of our computations, we find that d varies only a little as we move along the bifurcating curve $\mathscr{C}$. Furthermore, d does not vary much as a function of the vorticity $\omega = \gamma$.

The amplitude a is more interesting. We find that a is always monotonically increasing as we move along $\mathscr{C}$. The graph of a as a function of the bifurcation parameter Q provides a nice cartoon of $\mathscr{C}$ and we will often refer in subsequent sections of this paper to this depiction of a along $\mathscr{C}$ as if it were the bifurcating curve itself. In figure 3, four waves along $\mathscr{C}$ for a given vorticity ($\gamma = 2.95$) are represented as data points in this cartoon. The last data point along the bifurcating curve corresponds to a wave that is nearly stagnant. In figure 1, there are four surface profiles corresponding to waves that are the very last points along their computed bifurcating curves.

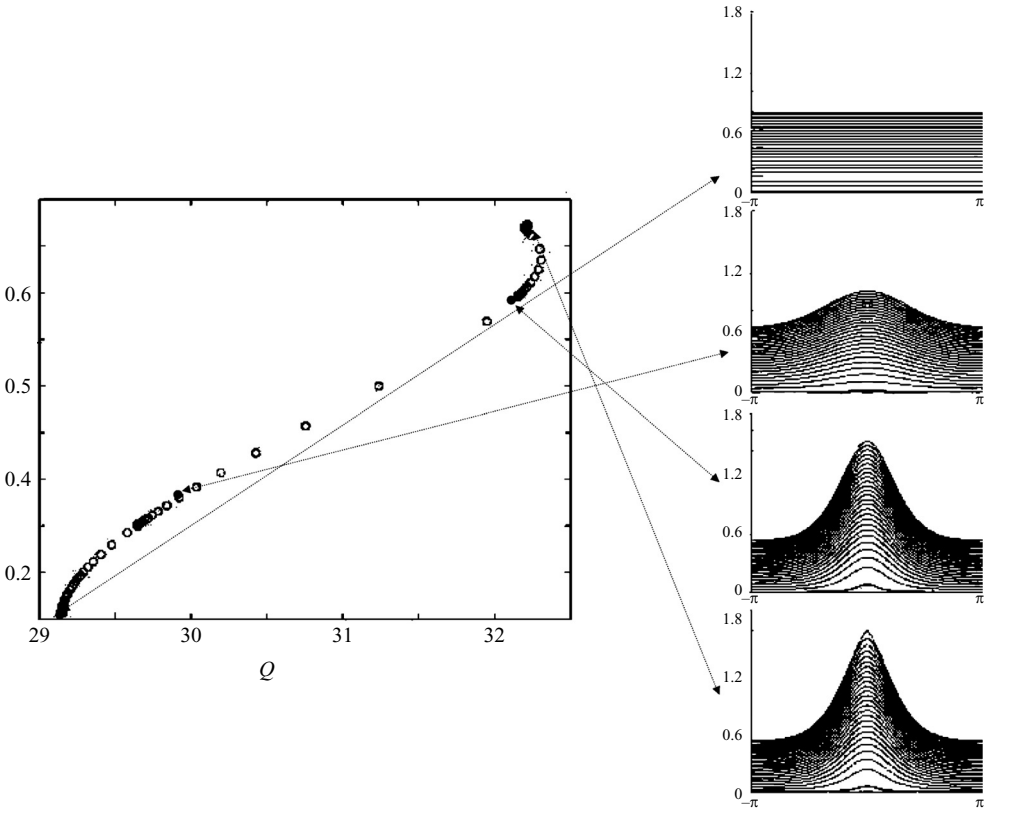

FIGURE 3. Each data point along the bifurcating curve represents a wave. At the right-hand side we show the wave shape and the streamlines for four waves along the bifurcation curve for $\gamma = 2.95$. The last point along the bifurcation curve corresponds to a wave near stagnation.

Since a is increasing along $\mathscr{C}$, the maximum amplitude a_{max} along the bifurcating curve occurs at the last computed point of $\mathscr{C}$. We can therefore investigate a_{max} as a function of γ. We find that a_{max} increases as a function of γ as long as $\gamma < \gamma_{crit}$. Thus, the maximum amplitude occurs for the extreme wave associated with $\gamma = \gamma_{crit}$. On the other hand, a_{max} decreases for $\gamma > \gamma_{crit}$. Figure 4 plots a_{max} as a function of γ. We see that a_{max} climbs to a sharp peak near γ_{crit} and then experiences a precipitous drop. In this case, $2.95 < \gamma_{crit} < 3$. In particular, note the very rapid dropoff of the amplitude from $\gamma = 2.95$ to the nearby value $\gamma = 3$ in figures 2 and 4. Also note that negative vorticity tends to lead to low-amplitude waves that stagnate at their crests. This may be interpreted to say that a favourable wind will lead to waves that break more easily.

In the course of many runs, we made various checks for other qualitative features of the bifurcating curve $\mathscr{C}$ itself. We find that the subcritical and supercritical cases separated by γ_{crit} seem to be further distinguished by the existence of a turning point in $\mathscr{C}$ where Q changes monotonicity (figure 2). For $\gamma < \gamma_{crit}$, there is a turning point in $\mathscr{C}$ and for $\gamma > \gamma_{crit}$ there is none. Notice that the turning point for $\gamma = -4$ occurs in the middle of $\mathscr{C}$, in contrast to the turning point occurring near stagnation for the other values of γ illustrated in figure 2. The case $\gamma = 3$ is supercritical and has no turning point.

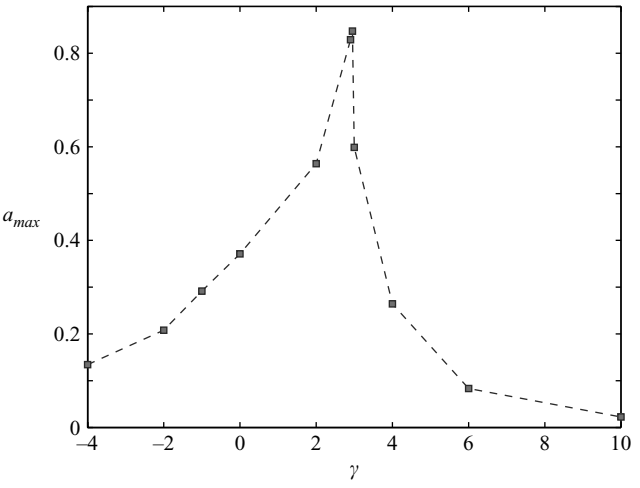

FIGURE 4. a_{max} for constant vorticity.

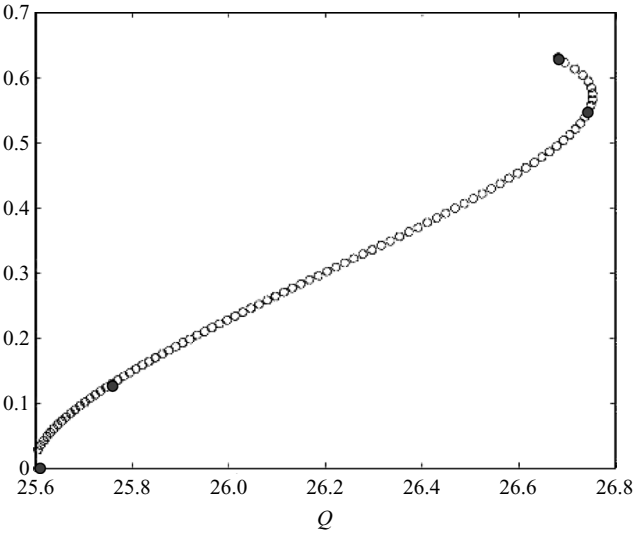

FIGURE 5. Amplitude plot for 10 % surface shear with shear value $\gamma_0 = 10$.

3. Surface shear

It is known experimentally that wind typically has the effect of producing vorticity in the water near the surface. In order to model this situation, we consider a shear vorticity layer of some uniform thickness $(|p_0|/100)\theta$ with respect to the streamfunction, below which the fluid is irrotational. Since the vorticity $\omega = \gamma(\psi)$ is necessarily constant on the streamlines, we therefore take $\gamma(\psi) = \gamma_0$ for $0 < \psi < (|p_0|/100)\theta$ and $\gamma(\psi) = 0$ for $(|p_0|/100)\theta < \psi < |p_0|$. Thus, θ is the percentage of fluid with vorticity γ_0.

Taking cues from our investigation of the constant vorticity case, we pay particular attention to the following characteristics of our computed waves: the location of first stagnation points, the shape of nearly stagnant waves, and the amplitude and depth of waves along the bifurcating curve up to stagnation. Figure 5 illustrates the bifurcating curve $\mathscr{C}$ and highlights four points along $\mathscr{C}$ for a 10 % shear layer ($\theta = 10$)

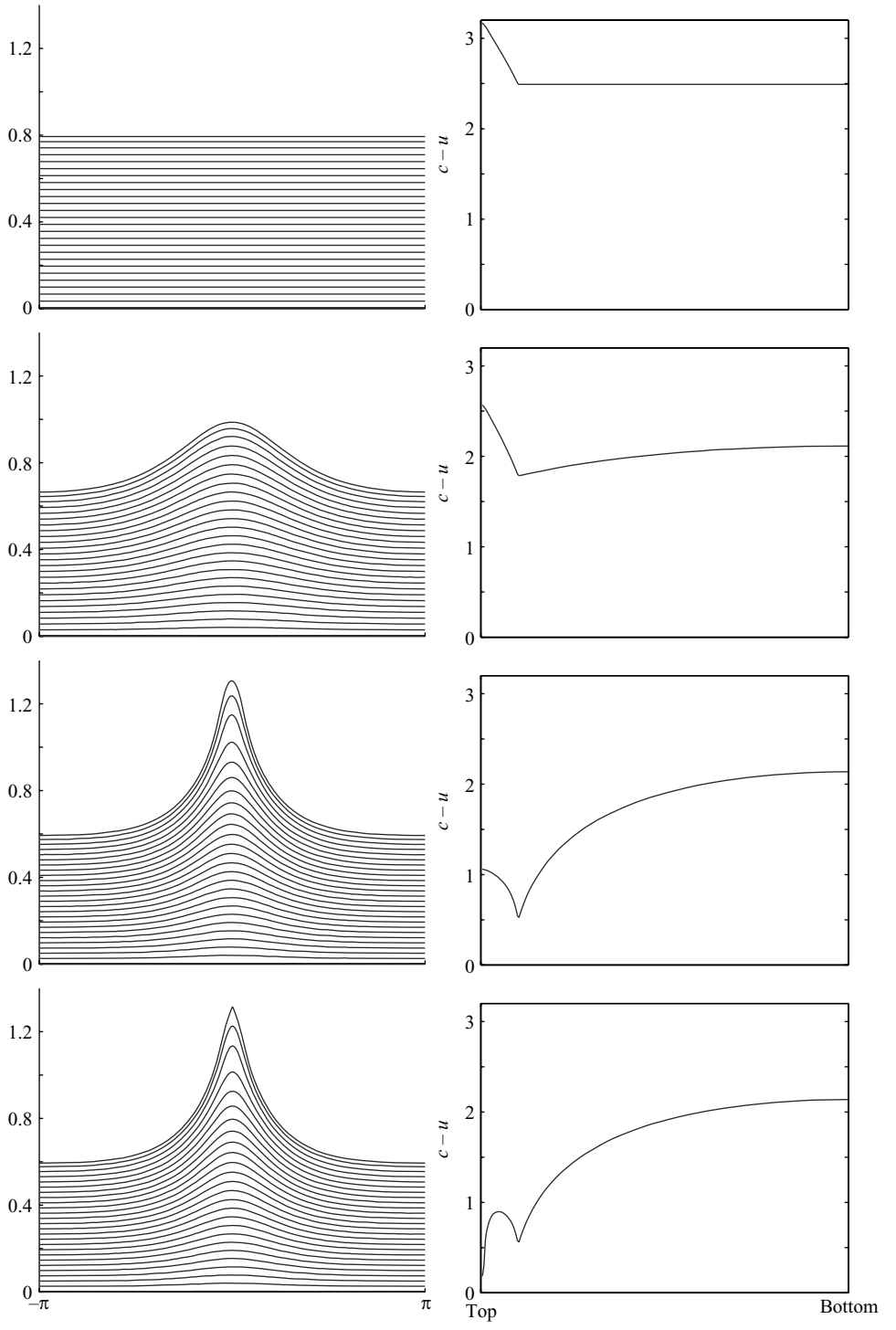

FIGURE 6. Four waves along $\mathscr{C}$ for a 10 % shear surface layer vorticity with $\gamma_0 = 10$.

with shear value $\gamma_0 = 10$. The corresponding waves are shown in figure 6. In this case, and in fact in all of our computations, we find that the first stagnation point always occurs along the line AB directly below the crest. The right-hand column of figure 6

$\theta\backslash\gamma_0$	−1	1	4	10	15	18	19	20	30	100
2	A	A	A	A	A	A	A	A	A	I
5	A	A	A	A	A	A	I	I	I	I
10	A	A	A	A	A	I	I	I	I	I
20	A	A	A	A	A	I	I	I	I	I
25	A	A	A	A	I	I	I	I	I	I
30	A	A	A	A	I	I	I	I	I	I
35	A	A	A	I	I	I	I	I	I	I
40	A	A	A	I	I	I	I	I	I	I
50	A	A	A	I	I	I	I	I	I	I
70	A	A	A	I	I	I	I	I	I	I
90	A	A	A	I	I	I	I	I	I	I
100	A	A	B	B	B	B	B	B	B	B

TABLE 1. Location of first stagnation points for waves with surface shear. They can occur at the crest (A), internally (I) or at the bottom (B) along the line below the crest depending on the thickness of the shear layer (θ) and the value of the vorticity in the layer (γ_0).

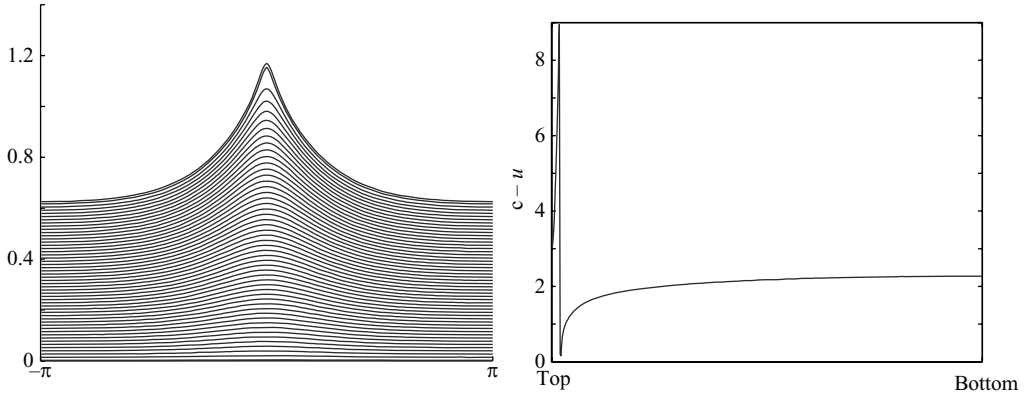

FIGURE 7. Internal stagnation occurs even for 2 % surface shear layer with $\gamma_0 = 100$.

plots the values of $c - u$ along this line for these four waves. Notice that only in the last instance along $\mathscr{C}$ does the crest A finally become close to stagnation.

Embarking on a more systematic treatment of this class of vorticities, we consider the location of the first stagnation point as a function of both the thickness θ of the layer and the magnitude γ_0 of the vorticity in that layer. As previously mentioned, we find that for all the vorticity functions that we consider, the first stagnation points occur along the line AB below the crest. In contrast to the constant vorticity case, however, we find that internal stagnation points can occur for such a variable vorticity. Whenever the first point of stagnation is internal, its exact position is the intersection of the streamline $\psi = (|p_0|/100)\theta$ with the vertical line through the crest. Many results are summarized in table 1. The case of constant vorticity, corresponding to the last row $\theta = 100$, is included for the sake of comparison. Negative vorticity always yields relatively small, peaky waves that stagnate at their crests.

We find that the location of first stagnation is at the crest (A) but that it becomes internal (I) as γ_0 becomes sufficiently large and positive and also (sometimes) as the layer becomes sufficiently thick. Figure 7 illustrates a wave with a very thin vorticity layer of very large shear (2 % layer, +100 shear) with an internal stagnation point.

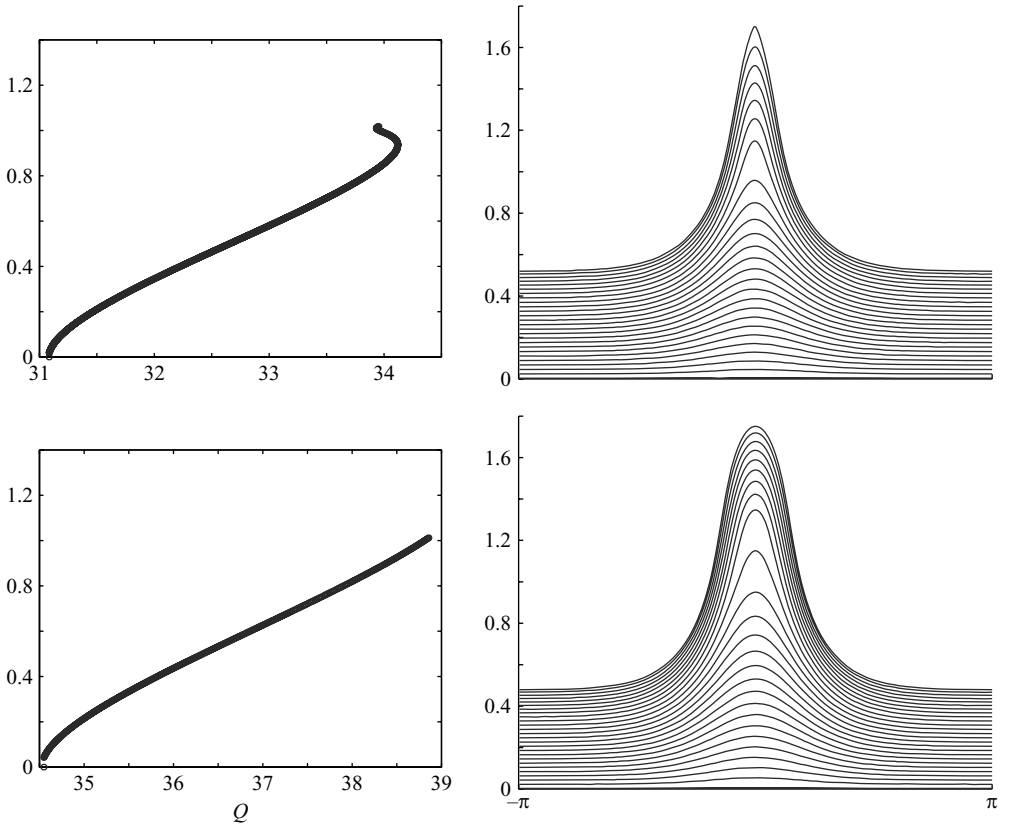

FIGURE 8. Surface shear. Top row: $\gamma_0 = 10, \theta = 25$, stagnation at the crest. Bottom row: $\gamma_0 = 10, \theta = 35$, internal stagnation.

We find that stagnation occurs at the bottom in the case of constant vorticity larger than $\gamma_{crit} \approx 2.95$.

Figure 8 illustrates two waves with $\gamma_0 = 10$, one with thickness 25 % that stagnates at the crest and the other with thickness 35 % that stagnates internally. These examples illustrate that some vorticity functions have bifurcating curves with turning points, and others have none. So far, we have not developed a general rule either to predict the presence of a turning point or to determine how many there are. Figures 2 and 8 suggest that the presence of a turning point is correlated with the occurrence of stagnation at the crest. Most of the bifurcating curves that we have encountered have either one turning point or none. However, figure 9, which illustrates $\mathscr{C}$ for $\theta = 5$, $\gamma_0 = 18$, has two turning points.

Next, we consider the amplitude a. We find the same general principles as in the constant vorticity case, namely, that a is monotonically increasing as we move along $\mathscr{C}$, but there is only a slight variation in d. Since a is always increasing along $\mathscr{C}$ up to the point of first stagnation, it is meaningful to compare a_{max}, the amplitude corresponding to the waves at the end of the computed bifurcating curve, as a function of vorticity. As is evident from table 1, we can consider a_{max} as a function of both γ_0 and θ. When we fix either one of these variables and consider a_{max} as a function of the other one (just restricting to any column or any row in table 1), we find that a_{max} increases as long as stagnation occurs at the crest, after which it decreases.

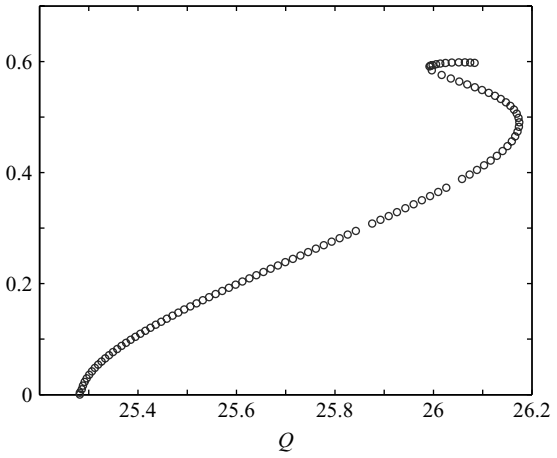

FIGURE 9. Amplitude plot for 5 % surface shear with shear value $\gamma_0 = 18$.

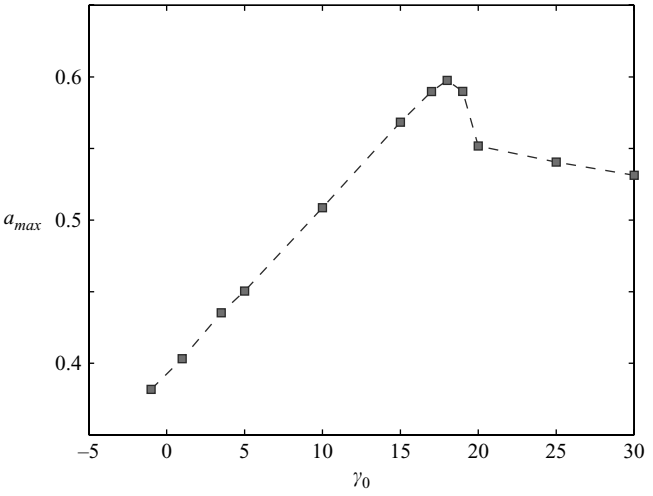

FIGURE 10. $a_{max}(\gamma_0)$ for 5 % shear surface layer.

Figure 10 plots a_{max} as a function of the shear value γ_0 for the row corresponding to $\theta = 5$ in table 1. Figure 11 plots a_{max} as a function of the thickness θ for the column corresponding to $\gamma_0 = 10$.

Figure 12 plots the near-extreme wave profiles for $\theta = 5$ and for $\gamma_0 = -1, +1, 18, 30$. We see that the amplitude increases and then decreases. Figure 13 plots the profiles for shear value $\gamma_0 = 10$ for various layer thicknesses $\theta = 5, 20, 30, 40, 90$. As we saw in table 1 and figure 11, the cases of $\theta = 40$ and 90 lead to internal stagnation and a modest decrease of amplitude. The wave profile evidently changes more dramatically as a function of the thickness θ of the shear layer than of the shear value γ_0.

4. Variable shear

We also consider three other classes of vorticities: bottom shear layers, middle shear layers and continuous shears. We report here only a few observations, leaving open the possibility of further systematic studies.

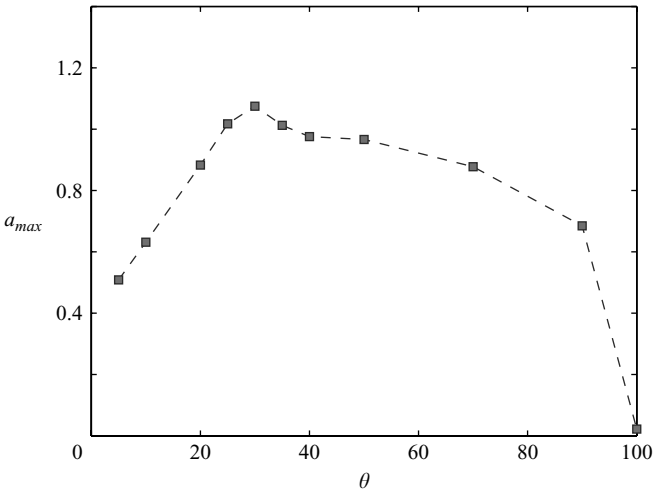

FIGURE 11. $a_{max}(\theta)$ for $\gamma_0 = 10$.

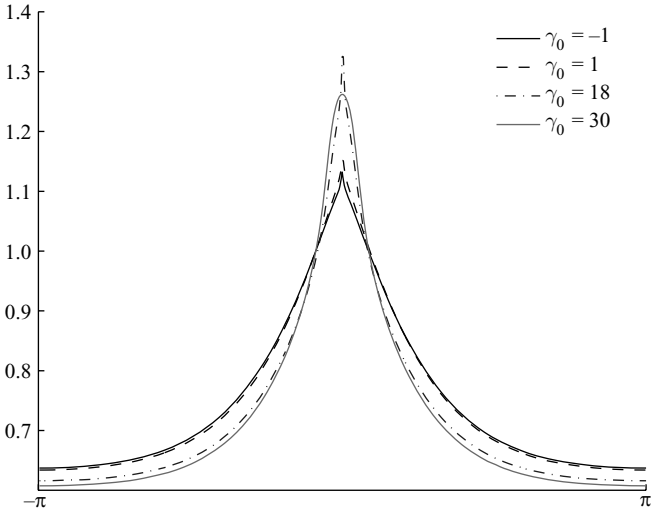

FIGURE 12. Wave profile as a function of shear value γ_0 for fixed surface-layer thickness $\theta = 5$.

For bottom shear layers, we consider a layer of some uniform thickness $(|p_0|/100)\theta_b$ with respect to the streamfunction, with a constant shear value γ_0 next to the bed, above which the fluid is irrotational. This situation might occur near the ocean shore, perhaps owing to tidal action. On the left-hand side of figure 14, we illustrate the case of a thin layer at the bed $\gamma_0 = 4, \theta_b = 10$ and on the right-hand side, a thick layer $\gamma_0 = 4, \theta_b = 65$. For $\gamma_0 = 4$, our computations (not all shown) yield first stagnation at the crest for $\theta_b \leqslant 60$ and at the bottom for larger θ_b. The streamline separation at the bottom is evident from figure 14 if $\theta = 65$. The study of waves that break at the bottom is important in sedimentation theory. These two locations, crest and bottom, are consistent with the analytical result in Constantin & Strauss (2007), which states that internal stagnation could never occur for a vorticity that increases with depth. The bifurcation diagrams are also illustrated in figure 14. The two cases are further

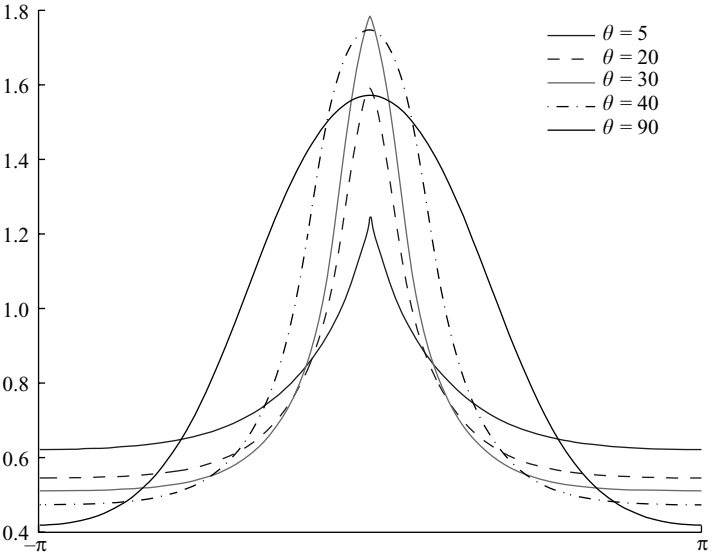

FIGURE 13. Wave profile as a function of surface-layer thickness θ for fixed shear value $\gamma_0 = 10$.

distinguished by the presence of a turning point in the bifurcation diagram for $\theta_b \leqslant 60$ and the absence of a turning point for larger θ_b. Notice also that for $\theta = 65$, there are a very large number of iterations (the circles overlapping so much that they appear to form a solid line in the bifurcation diagram) because the numerical problem is quite stiff.

We provide just one illustration of a middle shear layer in figure 15. We choose a thin layer of 5 % thickness located exactly in the middle of the basic interval $0 \leqslant \psi \leqslant |p_0|$ and a vorticity value $\gamma_0 = 10$. This vorticity function is obviously not monotone. The shear layer induces a rapid change in the value of the relative velocity $u - c$, as we can see from the right-hand side of figure 15. The illustration also shows that this wave stagnates at the crest.

Now we demonstrate the basic irrelevance of the discontinuities of the previous vorticity functions. For that purpose, we illustrate only the case of the continuous vorticity function $\gamma(p) = 10\tanh(10(p + 1))$. It is designed to yield an internal stagnation. Figure 16(a) shows the graph of vorticity *vs.* $p = -\psi$. It is rather steep, but because there are 500 mesh points, it is indeed a continuous distribution. Figure 16(b) illustrates the amplitude and depth along the bifurcating curve as a function of Q. Note the turning point near stagnation. Figure 16(c) is the wave itself with a very obvious separation of streamlines in the interior. Figure 16(d) shows that the wave is indeed very close to stagnation at middle depth.

5. Effect of the flux

In all of our previous computations the relative mass flux p_0 was taken to be $p_0 = -2$. In this section, we consider the effect of changing the value of the flux. We first select a simple comparison of surface shears for two values of p_0 to point out some general differences. Figure 17 shows the free surfaces of four waves near stagnation corresponding to surface shear vorticities given by shear thickness $\theta = 5\,\%$ and shear values $\gamma_0 = 1$ and 18 for both $p_0 = -2$ and $p_0 = -4$.

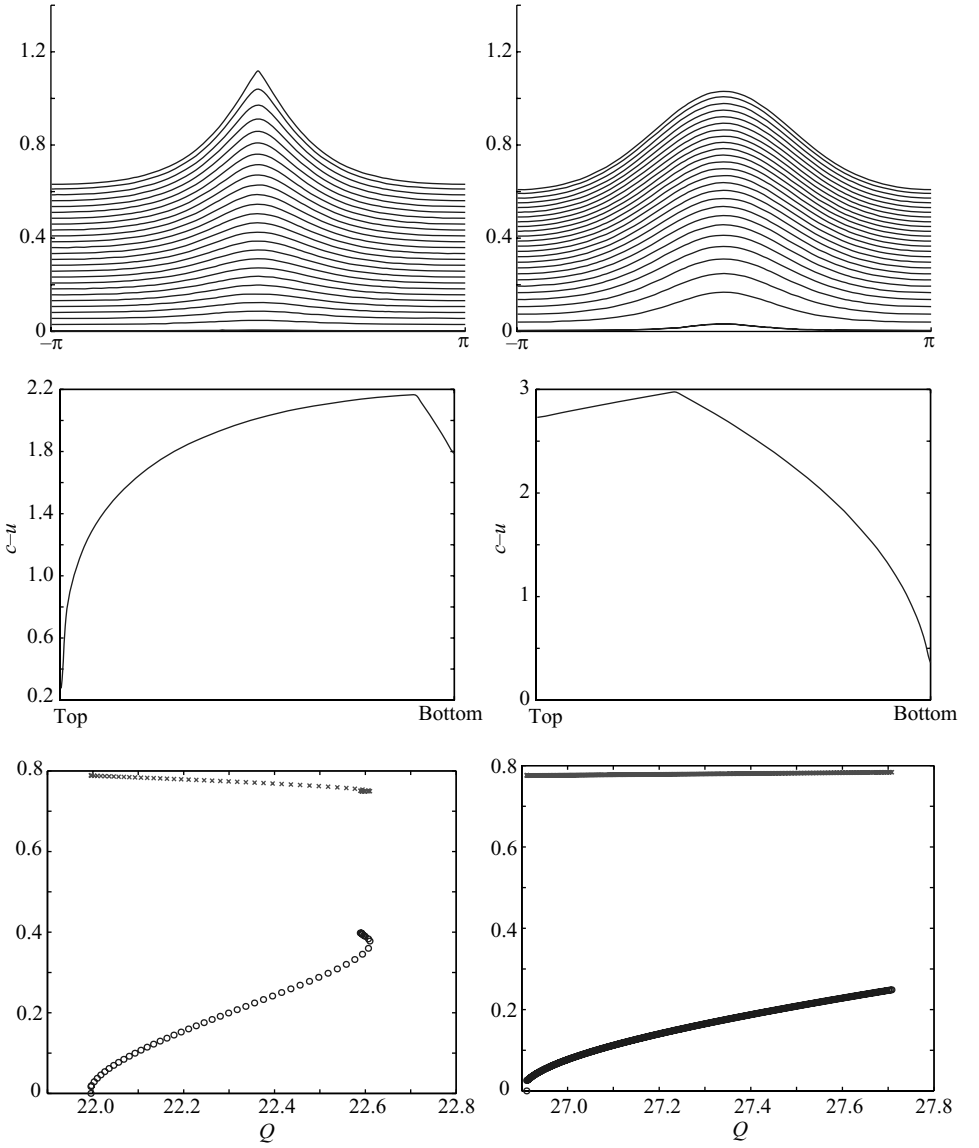

FIGURE 14. Bottom shear. Left-hand column: $\gamma_0 = 4, \theta_b = 10$; stagnation at the crest. Right-hand column: $\gamma_0 = 4, \theta_b = 65$; stagnation at the bottom below the crest. Second row: $c-u$ along vertical line AB. Third row: amplitude ($\circ$) and depth ($\times$) along $\mathscr{C}$ as functions of Q.

Immediately noticeable is the increase in depth d as we increase $|p_0|$. This is to be expected since an increase in $|p_0|$ translates to more fluid being transported in the fixed reference frame. Since the depth does not vary much along the bifurcating curve $\mathscr{C}$, the increase in depth as a function of $|p_0|$ is seen for all waves along $\mathscr{C}$. Next we consider the location of the stagnation point. Referring back to the second row of table 1, we see that if $p_0 = -2$ and $\theta = 5$, there is a value of the vorticity γ_0 between 18 and 19 that separates the case of first stagnation at the top and that at the bottom. The amplitude of the wave near stagnation is maximized at this critical value $\gamma_{0,crit}$.

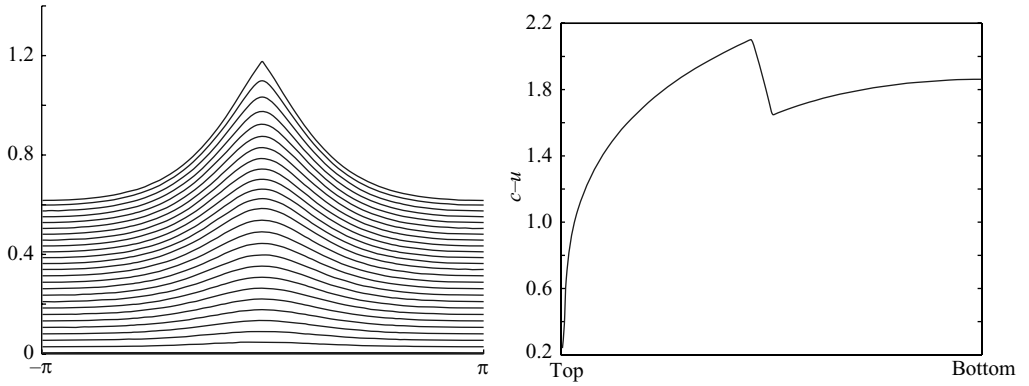

FIGURE 15. 5 % middle shear layer with shear value $\gamma_0 = 10$.

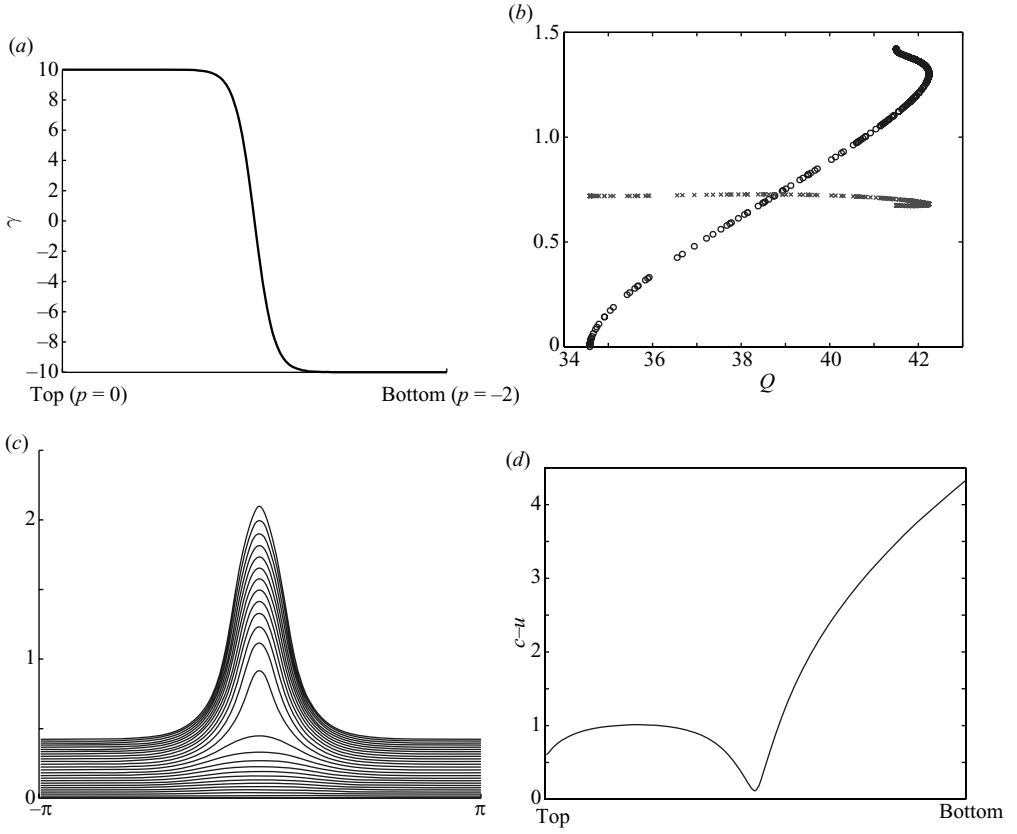

FIGURE 16. Continuous vorticity. (*a*) Graph of the continuous vorticity $\gamma(p) = 10\tanh 10(p+1)$; (*b*) amplitude (○) and depth (×) as functions of Q. (*c*) Wave streamlines, illustrating internal stagnation; (*d*) $c - u$ along the vertical line AB.

A similar statement can be made for a surface layer with $p_0 = -4$ by fixing $\theta = 5$ and varying γ_0. For $\gamma_0 = 1$, the first point of stagnation occurs at the top whereas for $\gamma_0 = 18$, this stagnation point occurs internally. Therefore the critical vorticity $\gamma_{0,crit}$ that separates the two cases of top stagnation and internal stagnation is smaller than 18.

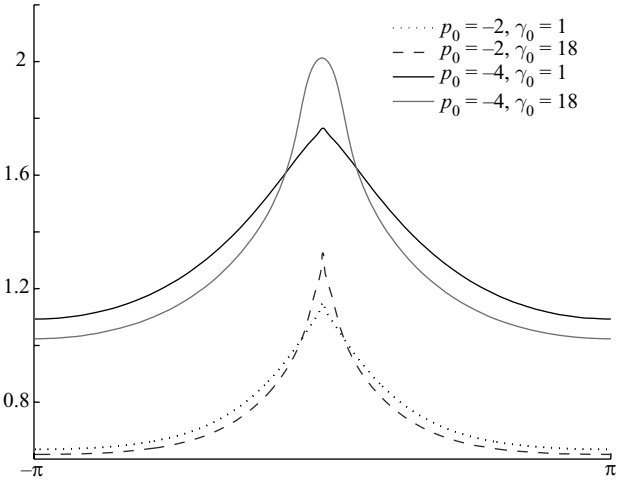

FIGURE 17. Surface streamlines for waves with surface shear vorticity for both $p_0 = -2$ and $p_0 = -4$.

These general observations hold for any value of p_0 as long as a bifurcating curve $\mathscr{C}$ exists for the class of vorticities in question. It is known from Constantin & Strauss (2004) that there might not exist a bifurcating curve at all, owing to the absence of any local bifurcation from laminar flow if $|p_0|$ and γ are too large. For general variable vorticity, there is an explicit condition that ensures the existence of local bifurcation. For surface shears with positive shear value γ_0 this sufficient condition for local bifurcation is that the following inequality is satisfied:

$$\int_{p_0\theta/100}^{0} \left\{ (p - p_0)^2 \left[2\gamma_0 \left(p - \frac{p_0\theta}{100} \right) \right]^{1/2} + \left[2\gamma_0 \left(p - \frac{p_0\theta}{100} \right) \right]^{3/2} \right\} \mathrm{d}p < g p_0^2. \tag{5.1}$$

There is a similar inequality for negative γ_0. The θ, γ_0 pairs given by $\theta = 5$ and $\gamma_0 = 1$ or 18 satisfy this sufficient condition for local bifurcation for both $p_0 = -2$ and $p_0 = -4$. However, our computations suggest that this condition (5.1) is far from being necessary. For $p_0 = -2$ and $\theta = 2\,\%$, for example, we have successfully found the existence of a bifurcating curve for shear values much larger than that given by (5.1), ending at the wave shown in figure 7.

For the case of constant positive vorticity γ, however, there is a necessary and sufficient condition for local bifurcation given by

$$\tanh \sqrt{\frac{2|p_0|}{\gamma}} \geqslant \frac{2|p_0|\gamma}{g + \gamma\sqrt{2|p_0|\gamma}}. \tag{5.2}$$

This case adequately illustrates the effect of the flux. Condition (5.2) is always satisfied for $p_0 = -2$ and constant $\gamma > 0$, which in turn ensures a bifurcating curve even for large γ. Varying p_0, we find that as $|p_0|$ increases, the range of positive γ for which the inequality is satisfied shrinks rapidly. For instance, when $p_0 = -4$, only $\gamma \leqslant 2.435$ satisfies this inequality; when $p_0 = -6$, the range reduces to $\gamma \leqslant 1.185$. In seeking γ_{crit} (the value of γ separating the cases where the location of the first stagnation occurs at the top or at the bottom) for larger values of p_0, we have on one hand a general observation that γ_{crit} should decrease as $|p_0|$ increases and on the other hand the

p_0	γ_{crit}	a_{max}
-1	3.25	0.54
-2	2.96	0.85
-3	2.55	0.98

TABLE 2. γ_{crit} and a_{max} as functions of p_0.

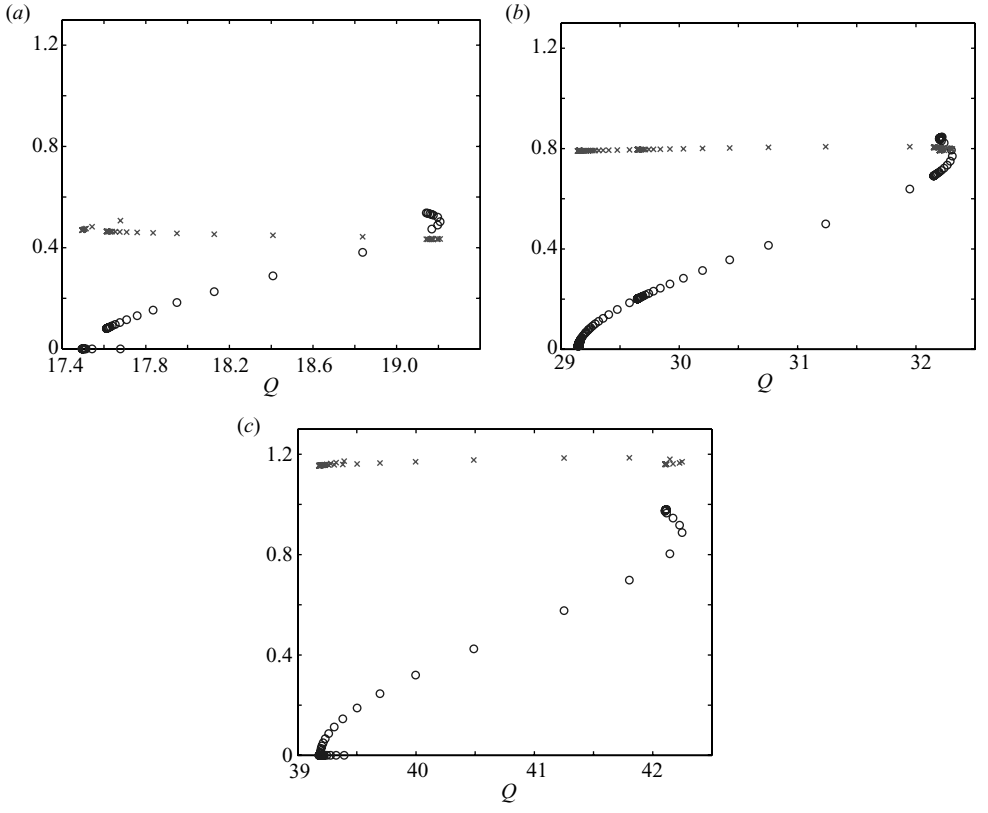

FIGURE 18. Amplitude (○) and depth (×) plots for $\gamma_{crit}(p_0)$. Both amplitude and depth increase as functions of $|p_0|$. (*a*) $R_0 = -1$, (*b*) -2, (*c*) -3.

precise upper bound (5.2) for γ beyond which there is no bifurcating curve at all. It is possible that γ_{crit} does not exist because stagnation occurs only at the crest.

In our computations, we are able to find a value for γ_{crit} for $|p_0| \leqslant 3$. For such p_0, the observations that we specified in the beginning of this section hold. Namely, we find that γ_{crit} is decreasing as a function of $|p_0|$; in this case, we find that $\gamma_{crit}(p_0 = -1) \approx 3.25$, $\gamma_{crit}(p_0 = -2) \approx 2.96$, and $\gamma_{crit}(p_0 = -3) \approx 2.55$. Furthermore, considering a_{max} as a function of $|p_0|$, we find that a_{max} is an increasing function of $|p_0|$ as seen in figure 18. Specifically, we find that $a_{max}(p_0 = -1) = 0.54$, $a_{max}(p_0 = -2) = 0.85$, and $a_{max}(p_0 = -3) = 0.98$. Thus, the tallest waves become taller as the flux of fluid increases, which is intuitively expected.

Several people were crucial to the success of this project. Our computer wizard, Joshua Bronson, set up the interface with Trilinos for us. Andrew Salinger of

Sandia National Laboratories generously lent us his expertise concerning Trilinos and numerical bifurcation. Adrian Constantin has been a close collaborator on the analytical aspects of water waves. Tetsu Hara has provided us with the perspective of the oceonography community.

REFERENCES

Benjamin, T. B. 1962 The solitary wave on a stream with an arbitrary distribution of vorticity. *J. Fluid Mech.* **12**, 97–116.

Constantin, A. & Escher, J. 2004 Symmetry of steady deep-water waves with vorticity. *Eur. J. Appl. Maths* **15**, 755–768.

Constantin, A. & Strauss, W 2004 Exact steady periodic water waves with vorticity. *Commun. Pure Appl. Maths* **57**, 481–527.

Constantin, A. & Strauss, W. 2007 Rotational steady water waves near stagnation. *Phil. Trans. R. Soc. Lond.* **365**, 2227–2239.

Dalrymple, R. A. 1977 A numerical model for periodic finite amplitude waves on a rotational fluid. *J. Comput. Phys.* **24**, 29–42.

Dubreil-Jacotin, M.-L. 1934 Sur la détermination rigoureuse des ondes permanentes périodiques d'ampleur finie. *J. Math. Pures Appl.* **13**, 217–291.

Hur, V. M. 2007 Symmetry of steady periodic surface water waves with vorticity. *Phil. Trans. R. Soc. Lond.* **365**, 2203–2214.

Johnson, R. S. 1997 *A Modern Introduction to the Mathematical Theory of Water Waves*. Cambridge University Press.

Ko, J. & Strauss, W. 2008 Large-amplitude steady rotational water waves. *Eur. J. Mech.*/B *Fluids* **27**, 96–109.

Lighthill, J. 2001 *Waves in Fluids*. Cambridge University Press.

Milne-Thomson, L. M. 1996 *Theoretical Hydrodynamics*. Dover.

Miroshnikov, V. A. 2002 The Boussinesq–Rayleigh approximation for rotational solitary waves on shallow water with uniform vorticity. *J. Fluid Mech.* **456**, 1–32.

Okamoto, H. & Shóji, M. 2001 *The Mathematical Theory of Permanent Progressive Water-Waves*. World Scientific.

Sha, H. & Vanden-Broeck, J.-M. 1995 Solitary waves on water of finite depth with a surface or bottom shear layer. *Phys. Fluids* **7**, 1048–1055.

Simmen, J. A. & Saffman, P. G. 1985 Steady deep-water waves on a linear shear current. *Stud. Appl. Maths* **73**, 35–57.

Swan, C., Cummins, I. P. & James, R. L. 2001 An experimental study of two-dimensional surface water waves propagating on depth-varying currents. Part 1. Regular waves. *J. Fluid Mech.* **428**, 273–304.

Teles da Silva, A. F. & Peregrine, D. H. 1988 Steep, steady surface waves on water of finite depth with constant vorticity. *J. Fluid Mech.* **195**, 281–302.

Thomas, G. P. 1990 Wavecurrent interactions: an experimental and numerical study. Part 2. Nonlinear waves. *J. Fluid Mech.* **216**, 505–536.

Vanden-Broeck, J.-M. 1994 Steep solitary waves in water of finite depth with constant vorticity. *J. Fluid Mech.* **274**, 339–348.

Vanden-Broeck, J.-M. 1995 New families of steep solitary waves in water of finite depth with constant vorticity. *Eur. J. Mech.* B *Fluids* **14**, 761–774.

Varvaruca, E. 2008 On some properties of travelling water waves with vorticity. *SIAM J. Math. Anal.* **39**, 1686–1692.